

UAV-Enabled Secure ISAC Against Dual Eavesdropping Threats: Joint Beamforming and Trajectory Design

Jianping Yao, *Member, IEEE*, Zeyu Yang, Zai Yang, *Senior Member, IEEE*,
Jie Xu, *Fellow, IEEE*, and Tony Q. S. Quek, *Fellow, IEEE*

Abstract—In this work, we study an unmanned aerial vehicle (UAV)-enabled secure integrated sensing and communication (ISAC) system, where a UAV serves as an aerial base station (BS) to simultaneously perform communication with a user and detect a target on the ground, while a dual-functional eavesdropper attempts to intercept the signals for both sensing and communication. Facing the dual eavesdropping threats, we aim to enhance the average achievable secrecy rate for the communication user by jointly designing the UAV trajectory together with the transmit information and sensing beamforming, while satisfying the requirements on sensing performance and sensing security, as well as the UAV power and flight constraints. To address the non-convex nature of the optimization problem, we employ the alternating optimization (AO) strategy, jointly with the successive convex approximation (SCA) and semidefinite relaxation (SDR) methods. Numerical results validate the proposed approach, demonstrating its ability to achieve a high secrecy rate while meeting the required sensing and security constraints.

Index Terms—Integrated sensing and communication (ISAC), unmanned aerial vehicle (UAV), physical-layer security, sensing security.

I. INTRODUCTION

Integrated sensing and communication (ISAC) is regarded as a promising cornerstone technology for future sixth-generation (6G) wireless networks to enable the joint sensing and communication operation in wireless networks [1], [2]. By allowing base stations (BSs) to transmit unified ISAC signals and perform ISAC signal processing over shared hardware platforms, ISAC is expected to significantly enhance the utilization efficiency of spectrum, hardware, and energy resources. Recently, with advancements in unmanned aerial vehicle (UAV) technology, the exploitation of UAVs has attracted growing interests to provide ISAC services from the sky, in which the controllable mobility in the three-dimensional (3D) space is utilized for UAVs to approach sensing targets and communication users to provide additional flexibility in enhancing the ISAC performance (see e.g., [3], [4]).

J. Yao and Z. Yang are with the School of Information Engineering, Guangdong University of Technology, Guangzhou 510006, China (E-mails: yaojp@gdut.edu.cn, yangzeyugdut@qq.com).

Z. Yang is with the School of Mathematics and Statistics, Xi'an Jiaotong University, Xi'an 710049, China (E-mail: yangzai@xjtu.edu.cn).

J. Xu is with the Future Network of Intelligence Institute (FNii) and the School of Science and Engineering, The Chinese University of Hong Kong, Shenzhen, Shenzhen 518172, China (E-mail: xujie@cuhk.edu.cn). J. Xu is the corresponding author.

T. Q. S. Quek is with Information Systems Technology and Design, Singapore University of Technology and Design, Singapore 487372, Singapore (E-mail: tonyquek@sutd.edu.sg).

Nevertheless, owing to the inherent broadcast characteristics of wireless transmission, the communication and sensing signals in ISAC systems are susceptible to interception, posing significant security challenges for both functionalities. To address communication security concerns, physical-layer security (PLS) has been proposed as an effective approach by leveraging the wireless channel properties, which has been extensively studied in prior research [5]. The core idea of these works is to propose an ISAC design to leverage artificial noise (AN) for not only interfering with the eavesdropper but also performing the target sensing, thus enhancing the communication security (see e.g., [6]–[8]).

On the other hand, there have been only a handful of prior works addressing the sensing security issue in ISAC systems. For instance, the work [9] considered a communication user acting as a sensing eavesdropper, in which the mutual information (MI) of the authorized sensing receiver is maximized via the joint beamforming design, while ensuring that the MI of the eavesdropper remains below a given threshold. Furthermore, the paper [10] was the first to jointly consider both PLS and sensing security by focusing on a secure cell-free ISAC system, where several ISAC transmitters collaboratively transmit confidential data to several legitimate communication receivers while conducting target detection under the threat of both communication and sensing eavesdroppers.

Different from prior works, this work studies a new UAV-enabled secure ISAC system. In this system, an aerial dual-functional BS delivers secure data to a legitimate communication receiver while simultaneously performing target sensing, and an eavesdropper attempts to intercept both the communication and sensing signals. Different from the conventional secure ISAC designs (e.g., [9], [10]), we exploit the UAV trajectory optimization together with the transmit information and sensing beamforming for enhancing the security performance. In particular, we maximize the average secrecy rate at the legitimate communication receiver, while ensuring the sensing performance requirements, subject to the UAV power and practical flight constraints, as well as the sensing security constraints. To tackle this non-convex problem, we develop an effective approach that leverages a combination of alternating optimization (AO), successive convex approximation (SCA), and semidefinite relaxation (SDR). Lastly, we provide numerical results to demonstrate the efficiency of the proposed method.

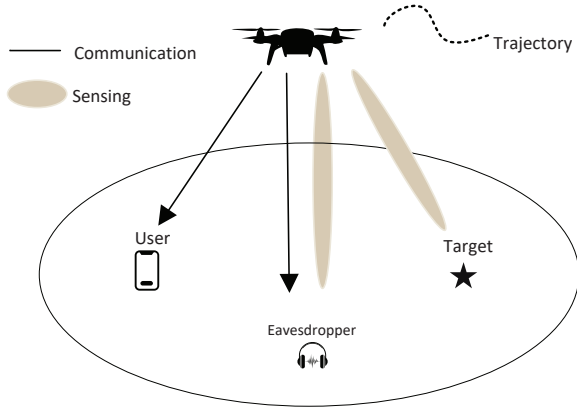


Fig. 1: Illustration of the UAV-enabled secure ISAC system.

II. SYSTEM MODEL

As shown in Fig. 1, we focus on a UAV-enabled secure ISAC system, where an aerial BS simultaneously transmits data to a legitimate communication user (denoted as u) and conducts wireless sensing towards a target (designated as t) on the ground, in the presence of a dual-functional eavesdropper (referred to as e) intercepting both communication and sensing information. We assume that the UAV is equipped with a uniform linear array (ULA) consisting of M antennas, arranged in a vertical orientation with respect to the horizontal plane with a constant altitude D . In contrast, all other nodes each have only one antenna. We consider a 3D Cartesian coordinate system, where the user, the target, and the eavesdropper on the ground with attitude 0 are fixed at horizontal locations $\mathbf{s}_u = (x_u, y_u)$, $\mathbf{s}_t = (x_t, y_t)$, and $\mathbf{s}_e = (x_e, y_e)$, respectively.

We consider a service duration T divided into N equal time slots, each with a duration of $t_s = T/N$. The time slot length is sufficiently short to ensure that the motion states of the UAV remain unchanged within each slot. Let $\mathcal{N} \triangleq \{1, \dots, N\}$ denote the collection of slots. Therefore, at slot $n \in \mathcal{N}$, we assume that the UAV's horizontal coordinate is $\boldsymbol{\rho}[n] = (x[n], y[n])$. Let $\boldsymbol{\rho}_I = (x_I, y_I)$ and $\boldsymbol{\rho}_F = (x_F, y_F)$ signify the starting and ending horizontal locations of the UAV. Let v_{\max} and $V_{\max} = v_{\max} t_s$ represent the maximum UAV speed and the maximum displacement within a single time slot, respectively. Consequently, we impose the following UAV flight constraints, given as

$$\boldsymbol{\rho}[1] = \boldsymbol{\rho}_I, \quad \boldsymbol{\rho}[N] = \boldsymbol{\rho}_F, \quad (1)$$

$$\|\boldsymbol{\rho}[n+1] - \boldsymbol{\rho}[n]\| \leq V_{\max}, \quad \forall n \in \mathcal{N}. \quad (2)$$

Let $a_i[n]$ represent the intended communication signal for the user at slot n , $\mathbf{b}[n] \in \mathbb{C}^{M \times 1}$ denote the associated transmit beamforming vector, and $\mathbf{a}_s[n] \in \mathbb{C}^{M \times 1}$ denote the specific wireless sensing signal at slot n , which simultaneously serves as AN to interfere with the eavesdropper. We assume that the communication signal $a_i[n]$ is independently drawn from a circularly symmetric complex Gaussian (CSCG) distribution. Additionally, the wireless sensing signal $\mathbf{a}_s[n]$ is treated as an independently random vector with a mean of zero and a covariance matrix $\mathbf{A}_s[n] = \mathbb{E}[\mathbf{a}_s[n]\mathbf{a}_s^H[n]] \succeq \mathbf{0}$ [3], where

$\mathbb{E}(\cdot)$ denotes the expectation operator and $\mathbf{a}_s^H[n]$ represents its conjugate transpose.

At each slot $n \in \mathcal{N}$, we denote $\Phi_o(\boldsymbol{\rho}[n])$, $o \in \{u, e, t\}$, as the steering vector associated with the UAV at location $\boldsymbol{\rho}[n]$ towards ground node o as

$$\Phi_o(\boldsymbol{\rho}[n]) = [\phi_{o1}[n], \dots, \phi_{om}[n], \dots, \phi_{oM}[n]]^T, \quad (3)$$

where $\phi_{om}[n] = e^{j2\pi \frac{k}{\lambda}(m-1) \cos \theta_o(\boldsymbol{\rho}[n])}$; $\theta_o(\boldsymbol{\rho}[n]) = \arccos \frac{D}{\sqrt{\|\boldsymbol{\rho}[n] - \mathbf{s}_o\|^2 + D^2}}$ denotes the angle of departure (AoD) associated with the location \mathbf{s}_o ; λ refers to the carrier wavelength; $k = \lambda/2$ indicates the distance between two adjacent antennas. Then, the channel vector between the UAV and node $o \in \{u, e, t\}$ at slot $n \in \mathcal{N}$ is given as

$$\mathbf{g}_o(\boldsymbol{\rho}[n]) = \sqrt{\frac{\beta_0}{d_o^2(\boldsymbol{\rho}[n])}} \Phi_o(\boldsymbol{\rho}[n]), \quad (4)$$

where β_0 represents the channel power gain at a reference distance of 1 meter, $d_o(\boldsymbol{\rho}[n]) = \sqrt{\|\boldsymbol{\rho}[n] - \mathbf{s}_o\|^2 + D^2}$ is the distance from the UAV to the location \mathbf{s}_o .

Accordingly, the received signal at location \mathbf{s}_o , $o \in \{u, e, t\}$ at slot $n \in \mathcal{N}$ is expressed as

$$z_o[n] = \mathbf{g}_o^H(\boldsymbol{\rho}[n])(\mathbf{b}[n]a_i[n] + \mathbf{a}_s[n]) + v_o[n], \quad (5)$$

where $v_o[n]$ represents the additive white Gaussian noise (AWGN) at the location \mathbf{s}_o 's receiver, characterized as a CSCG random variable with a mean of zero and a variance of σ^2 .

The received signal-to-interference-plus-noise ratio (SINR) at the user and the eavesdropper at slot n are respectively given as

$$\gamma_u[n] = \frac{|\mathbf{g}_u^H(\boldsymbol{\rho}[n])\mathbf{b}[n]|^2}{\mathbf{g}_u^H(\boldsymbol{\rho}[n])\mathbf{A}_s[n]\mathbf{g}_u(\boldsymbol{\rho}[n]) + \sigma^2}, \quad (6)$$

$$\gamma_e[n] = \frac{|\mathbf{g}_e^H(\boldsymbol{\rho}[n])\mathbf{b}[n]|^2}{\mathbf{g}_e^H(\boldsymbol{\rho}[n])\mathbf{A}_s[n]\mathbf{g}_e(\boldsymbol{\rho}[n]) + \sigma^2}. \quad (7)$$

Then, the achievable rates from the UAV to the user and the eavesdropper (in bps/Hz) at slot n are formulated as

$$R_u[n] = \log_2(1 + \gamma_u[n]), \quad (8)$$

$$R_e[n] = \log_2(1 + \gamma_e[n]). \quad (9)$$

Consequently, the secrecy rate from the UAV to the user at slot n is [5]

$$R_s[n] = [\log_2(1 + \gamma_u[n]) - \log_2(1 + \gamma_e[n])]^+, \quad (10)$$

where $[u]^+ \triangleq \max(u, 0)$.

In the considered ISAC system, the UAV intends to detect the target. To properly illuminate the target, the transmit beam pattern gain $\zeta_t[n]$ at the specified sensing location must meet a threshold Γ_t , which is proportional to the square of the distance between the UAV and the target, given as [3], [11]

$$\begin{aligned} \zeta_t[n] &= \mathbb{E}[|\Phi_t^H(\boldsymbol{\rho}[n])(\mathbf{b}[n]a_i[n] + \mathbf{a}_s[n])|^2] \\ &= \Phi_t^H(\boldsymbol{\rho}[n])(\mathbf{b}[n]\mathbf{b}^H[n] + \mathbf{A}_s[n])\Phi_t(\boldsymbol{\rho}[n]) \\ &\geq \Gamma_t d_t^2(\boldsymbol{\rho}[n]), \quad \forall n \in \mathcal{N}. \end{aligned} \quad (11)$$

Similarly, to ensure sensing security, the transmit beam pattern gain $\zeta_e[n]$ at the eavesdropper should not exceed a specific threshold Γ_e , which is proportional to the square of

the distance between the UAV and the eavesdropper, given as [3], [11]

$$\begin{aligned}\zeta_e[n] &= \mathbb{E}[|\Phi_e^H(\boldsymbol{\rho}[n])(\mathbf{b}[n]a_i[n] + \mathbf{a}_s[n])|^2] \\ &= \Phi_e^H(\boldsymbol{\rho}[n])(\mathbf{b}[n]\mathbf{b}^H[n] + \mathbf{A}_s[n])\Phi_e(\boldsymbol{\rho}[n]) \\ &\leq \Gamma_e d_e^2(\boldsymbol{\rho}[n]), \forall n \in \mathcal{N}.\end{aligned}\quad (12)$$

This study focuses on the joint optimization of the communication beamforming vectors $\{\mathbf{b}[n]\}$, the sensing covariance matrices $\{\mathbf{A}_s[n]\}$, and the UAV trajectory $\{\boldsymbol{\rho}[n]\}$ to maximize the average secrecy rate, subject to sensing security constraints, sensing constraints, power constraints, and UAV trajectory constraints. The problem is formulated as

$$\begin{aligned}(\text{P1}) : \quad & \max_{\{\mathbf{b}[n], \mathbf{A}_s[n], \boldsymbol{\rho}[n]\}} \frac{1}{N} \sum_{n=1}^N R_s[n] \\ \text{s.t.} \quad & \boldsymbol{\rho}[1] = \boldsymbol{\rho}_I, \boldsymbol{\rho}[N] = \boldsymbol{\rho}_F, \quad (13a) \\ & \|\boldsymbol{\rho}[n+1] - \boldsymbol{\rho}[n]\| \leq V_{\max}, \forall n \in \mathcal{N}, \quad (13b) \\ & \zeta_t[n] \geq \Gamma_t d_t^2(\boldsymbol{\rho}[n]), \forall n \in \mathcal{N}, \quad (13c) \\ & \zeta_e[n] \leq \Gamma_e d_e^2(\boldsymbol{\rho}[n]), \forall n \in \mathcal{N}, \quad (13d) \\ & \|\mathbf{b}[n]\|^2 + \text{tr}(\mathbf{A}_s[n]) \leq P_{\max}, \forall n \in \mathcal{N}, \quad (13e)\end{aligned}$$

where P_{\max} represents the UAV's maximum allowable power level. Since the objective function, along with constraints (13c) and (13d) are non-convex, problem (P1) is inherently challenging to be solved directly.

III. PROPOSED SOLUTION

This section presents an effective approach for solving problem (P1) by leveraging convex optimization, SDR, and SCA techniques.

A. Optimization of Information and Sensing Beamforming

We first address the optimization of the communication beamforming vectors $\{\mathbf{b}[n]\}$ and the sensing covariance matrices $\{\mathbf{A}_s[n]\}$ while keeping the UAV trajectory $\{\boldsymbol{\rho}[n]\}$ fixed. Under this consideration, problem (P1) is simplified to

$$\begin{aligned}(\text{P2}) : \quad & \max_{\{\mathbf{b}[n], \mathbf{A}_s[n]\}} \frac{1}{N} \sum_{n=1}^N R_s[n] \\ \text{s.t.} \quad & (13c), (13d), \text{ and } (13e).\end{aligned}$$

We define $\mathbf{B}[n] = \mathbf{b}[n]\mathbf{b}^H[n]$ such that $\text{rank}(\mathbf{B}[n]) \leq 1$ and $\mathbf{B}[n] \succeq \mathbf{0}$. Then problem (P2) is equivalently transformed as

$$\begin{aligned}(\text{P3}) : \quad & \max_{\{\mathbf{b}[n], \mathbf{A}_s[n]\}} \frac{1}{N} \sum_{n=1}^N (R_u[n] - R_e[n]) \\ \text{s.t.} \quad & \text{rank}(\mathbf{B}[n]) \leq 1, \mathbf{B}[n] \succeq \mathbf{0}, \forall n \in \mathcal{N}, \quad (14a)\end{aligned}$$

$$\begin{aligned}\Phi_t^H(\boldsymbol{\rho}[n])(\mathbf{B}[n] + \mathbf{A}_s[n])\Phi_t(\boldsymbol{\rho}[n]) \\ \geq \Gamma_t d_t^2(\boldsymbol{\rho}[n]), \forall n \in \mathcal{N}, \quad (14b)\end{aligned}$$

$$\begin{aligned}\Phi_e^H(\boldsymbol{\rho}[n])(\mathbf{B}[n] + \mathbf{A}_s[n])\Phi_e(\boldsymbol{\rho}[n]) \\ \leq \Gamma_e d_e^2(\boldsymbol{\rho}[n]), \forall n \in \mathcal{N}, \quad (14c)\end{aligned}$$

$$\text{tr}(\mathbf{B}[n]) + \text{tr}(\mathbf{A}_s[n]) \leq P_{\max}, \forall n \in \mathcal{N}. \quad (14d)$$

Problem (P3) remains non-convex due to the non-concave objective function and the rank-one constraint. To address

this, we apply the SDR approach by omitting the rank-one constraint in (14a). Subsequently, we handle the non-concave objective function of problem (P3) by applying the SCA technique to achieve a convergent solution iteratively. At each iteration $l \geq 1$, we derive a lower bound of the objective function under given local point $\mathbf{B}^{(l)}[n]$ and $\mathbf{A}_s^{(l)}[n]$ through the first-order Taylor expansion, given as

$$\begin{aligned}\hat{R}^{(l)}[n] &\triangleq \log_2(\text{tr}(\mathbf{g}_u(\boldsymbol{\rho}[n])\mathbf{g}_u^H(\boldsymbol{\rho}[n])\mathbf{B}[n]) \\ &+ \text{tr}(\mathbf{g}_u(\boldsymbol{\rho}[n])\mathbf{g}_u^H(\boldsymbol{\rho}[n])\mathbf{A}_s[n]) + \sigma^2) \\ &+ \log_2(\text{tr}(\mathbf{g}_e(\boldsymbol{\rho}[n])\mathbf{g}_e^H(\boldsymbol{\rho}[n])\mathbf{A}_s[n]) + \sigma^2) \\ &- (\delta_u^{(l)}[n] + \text{tr}(\Lambda_u^{(l)}[n](\mathbf{A}_s[n] - \mathbf{A}_s^{(l)}[n]))) \\ &- (\delta_e^{(l)}[n] + \text{tr}(\Lambda_e^{(l)}[n](\mathbf{B}[n] - \mathbf{B}^{(l)}[n])) \\ &+ \text{tr}(\Lambda_e^{(l)}[n](\mathbf{A}_s[n] - \mathbf{A}_s^{(l)}[n])),\end{aligned}\quad (15)$$

where

$$\delta_u^{(l)}[n] = \log_2(\text{tr}(\mathbf{g}_u(\boldsymbol{\rho}[n])\mathbf{g}_u^H(\boldsymbol{\rho}[n])\mathbf{A}_s^{(l)}[n]) + \sigma^2), \quad (16)$$

$$\Lambda_u^{(l)}[n] = \frac{\log_2 e \mathbf{g}_u(\boldsymbol{\rho}[n])\mathbf{g}_u^H(\boldsymbol{\rho}[n])}{\text{tr}(\mathbf{g}_u(\boldsymbol{\rho}[n])\mathbf{g}_u^H(\boldsymbol{\rho}[n])\mathbf{A}_s^{(l)}[n]) + \sigma^2}, \quad (17)$$

$$\begin{aligned}\delta_e^{(l)}[n] &= \log_2(\text{tr}(\mathbf{g}_e(\boldsymbol{\rho}[n])\mathbf{g}_e^H(\boldsymbol{\rho}[n])\mathbf{B}^{(l)}[n]) \\ &+ \text{tr}(\mathbf{g}_e(\boldsymbol{\rho}[n])\mathbf{g}_e^H(\boldsymbol{\rho}[n])\mathbf{A}_s^{(l)}[n]) + \sigma^2),\end{aligned}\quad (18)$$

$$\begin{aligned}\Lambda_e^{(l)}[n] &= (\log_2 e \mathbf{g}_e(\boldsymbol{\rho}[n])\mathbf{g}_e^H(\boldsymbol{\rho}[n])) \\ &\div (\text{tr}(\mathbf{g}_e(\boldsymbol{\rho}[n])\mathbf{g}_e^H(\boldsymbol{\rho}[n])\mathbf{B}^{(l)}[n]) \\ &+ \text{tr}(\mathbf{g}_e(\boldsymbol{\rho}[n])\mathbf{g}_e^H(\boldsymbol{\rho}[n])\mathbf{A}_s^{(l)}[n]) + \sigma^2).\end{aligned}\quad (19)$$

Consequently, we approximate problem (P3) as a convex problem and solve it iteratively.

Lemma 1: With the converged solution $\mathbf{B}^*[n]$ and $\mathbf{A}_s^*[n]$ obtained by the SCA technique, we can always construct an alternative solution satisfying the rank-one constraint, shown as follows

$$\bar{\mathbf{b}}[n] = \frac{\mathbf{B}^*[n]\mathbf{g}_u(\boldsymbol{\rho}[n])}{\sqrt{\mathbf{g}_u^H(\boldsymbol{\rho}[n])\mathbf{B}^*[n]\mathbf{g}_u(\boldsymbol{\rho}[n])}}, \quad (20)$$

$$\bar{\mathbf{B}}[n] = \bar{\mathbf{b}}[n]\bar{\mathbf{b}}^H[n], \quad (21)$$

$$\bar{\mathbf{A}}_s[n] = \mathbf{B}^*[n] + \mathbf{A}_s^*[n] - \bar{\mathbf{B}}[n], \quad (22)$$

where $\text{rank}(\bar{\mathbf{B}}[n]) = 1$.

Proof 1: See Appendix A.

B. UAV Trajectory Optimization

With the information and sensing beamforming $\{\mathbf{b}[n]\}$ and $\{\mathbf{A}_s[n]\}$ fixed, we proceed to optimize the UAV trajectory $\{\boldsymbol{\rho}[n]\}$, for which problem (P1) is reduced to

$$(\text{P4}) : \max_{\{\boldsymbol{\rho}[n]\}} \frac{1}{N} \sum_{n=1}^N R_s[n]$$

$$\text{s.t.} \quad \Phi_t^H(\boldsymbol{\rho}[n])\mathbf{E}[n]\Phi_t(\boldsymbol{\rho}[n]) \geq \Gamma_t d_t^2(\boldsymbol{\rho}[n]), \forall n \in \mathcal{N}, \quad (23a)$$

$$\Phi_e^H(\boldsymbol{\rho}[n])\mathbf{E}[n]\Phi_e(\boldsymbol{\rho}[n]) \leq \Gamma_e d_e^2(\boldsymbol{\rho}[n]), \forall n \in \mathcal{N}, \quad (23b)$$

$$(1) \text{ and } (2),$$

$$\eta_o(\mathbf{E}[n], \boldsymbol{\rho}[n]) = \sum_{p=1}^M [\mathbf{E}[n]]_{p,p} + 2 \sum_{i=1}^M \sum_{j=i+1}^M |[\mathbf{E}[n]]_{i,j}| \cos(\theta_{i,j}^{\mathbf{E}}[n] + \frac{\pi(j-i)D}{d_o(\boldsymbol{\rho}[n])}) + \frac{\sigma^2}{\beta_0} d_o^2(\boldsymbol{\rho}[n]), o \in \{u, e, t\}. \quad (27)$$

$$\xi_o(\mathbf{A}_s[n], \boldsymbol{\rho}[n]) = \sum_{p=1}^M [\mathbf{A}_s[n]]_{p,p} + 2 \sum_{i=1}^M \sum_{j=i+1}^M |[\mathbf{A}_s[n]]_{i,j}| \cos(\theta_{i,j}^{\mathbf{A}_s}[n] + \frac{\pi(j-i)D}{d_o(\boldsymbol{\rho}[n])}) + \frac{\sigma^2}{\beta_0} d_o^2(\boldsymbol{\rho}[n]), o \in \{u, e, t\}. \quad (28)$$

where $\mathbf{E}[n] = \mathbf{b}[n]\mathbf{b}^H[n] + \mathbf{A}_s[n]$ is introduced for notational convenience. Consequently, we represent the elements in the i -th row and j -th column of $\mathbf{B}[n]$, $\mathbf{A}_s[n]$, and $\mathbf{E}[n]$ as $[\mathbf{B}[n]]_{i,j}$, $[\mathbf{A}_s[n]]_{i,j}$, and $[\mathbf{E}[n]]_{i,j}$, where their magnitudes are denoted by $|[\mathbf{B}[n]]_{i,j}|$, $|[\mathbf{A}_s[n]]_{i,j}|$, and $|[\mathbf{E}[n]]_{i,j}|$ and their phases are denoted by $\theta_{i,j}^{\mathbf{B}}[n]$, $\theta_{i,j}^{\mathbf{A}_s}[n]$, and $\theta_{i,j}^{\mathbf{E}}[n]$, respectively. Problem (P4) is non-convex due to the non-convexity of the objective function in (P4), constraints (23a), and (23b). To address this, we rewrite the non-concave objective function and constraints as

$$R_s[n] = \log_2(\eta_u(\mathbf{E}[n], \boldsymbol{\rho}[n])) + \log_2(\xi_e(\mathbf{A}_s[n], \boldsymbol{\rho}[n])) - \log_2(\xi_u(\mathbf{A}_s[n], \boldsymbol{\rho}[n])) - \log_2(\eta_e(\mathbf{E}[n], \boldsymbol{\rho}[n])), \quad (24)$$

$$\Xi_t(\mathbf{E}[n], \boldsymbol{\rho}[n])/d_t^2(\boldsymbol{\rho}[n]) \geq \Gamma_t, \quad (25)$$

$$\Xi_e(\mathbf{E}[n], \boldsymbol{\rho}[n])/d_e^2(\boldsymbol{\rho}[n]) \leq \Gamma_e, \quad (26)$$

where $\eta_u(\mathbf{E}[n], \boldsymbol{\rho}[n])$, $\xi_u(\mathbf{A}_s[n], \boldsymbol{\rho}[n])$, $\eta_e(\mathbf{E}[n], \boldsymbol{\rho}[n])$, $\xi_e(\mathbf{A}_s[n], \boldsymbol{\rho}[n])$, and $\eta_t(\mathbf{E}[n], \boldsymbol{\rho}[n])$ are shown in (27) and (28), respectively; $\Xi_o(\mathbf{E}[n], \boldsymbol{\rho}[n]) = \eta_o(\mathbf{E}[n], \boldsymbol{\rho}[n]) - \frac{\sigma^2}{\beta_0} d_o^2(\boldsymbol{\rho}[n]), o \in \{u, e, t\}$.

Next, we introduce the trust-region-based SCA method, which is executed iteratively. Considering a specific iteration l with a local trajectory point $\boldsymbol{\rho}^{(l)}[n]$, we approximate (24), (25), and (26) applying the first-order Taylor expansion as

$$\bar{R}_s^{(l)}[n] \triangleq \log_2(\eta_u(\mathbf{E}[n], \boldsymbol{\rho}^{(l)}[n])) - \log_2(\xi_u(\mathbf{A}_s[n], \boldsymbol{\rho}^{(l)}[n])) - (\log_2(\eta_e(\mathbf{E}[n], \boldsymbol{\rho}^{(l)}[n])) - \log_2(\xi_e(\mathbf{A}_s[n], \boldsymbol{\rho}^{(l)}[n]))) + (\boldsymbol{\rho}_u^{(l)H}[n] - \boldsymbol{\rho}_e^{(l)H}[n])(\boldsymbol{\rho}[n] - \boldsymbol{\rho}^{(l)}[n]), \quad (29)$$

$$\frac{\Xi_t(\mathbf{E}[n], \boldsymbol{\rho}^{(l)}[n])}{d_t^2(\boldsymbol{\rho}^{(l)}[n])} + \frac{\tau_t^{(l)}[n]d_t^2(\boldsymbol{\rho}^{(l)}[n]) - 2\Xi_t(\mathbf{E}[n], \boldsymbol{\rho}^{(l)}[n])(\boldsymbol{\rho}^{(l)}[n] - \mathbf{s}_t)}{d_t^4(\boldsymbol{\rho}^{(l)}[n])} \times (\boldsymbol{\rho}[n] - \boldsymbol{\rho}^{(l)}[n]) \geq \Gamma_t, \quad (30)$$

$$\frac{\Xi_e(\mathbf{E}[n], \boldsymbol{\rho}^{(l)}[n])}{d_e^2(\boldsymbol{\rho}^{(l)}[n])} + \frac{\tau_e^{(l)}[n]d_e^2(\boldsymbol{\rho}^{(l)}[n]) - 2\Xi_e(\mathbf{E}[n], \boldsymbol{\rho}^{(l)}[n])(\boldsymbol{\rho}^{(l)}[n] - \mathbf{s}_e)}{d_e^4(\boldsymbol{\rho}^{(l)}[n])} \times (\boldsymbol{\rho}[n] - \boldsymbol{\rho}^{(l)}[n]) \leq \Gamma_e, \quad (31)$$

where $\boldsymbol{\rho}_u^{(l)}[n]$, $\boldsymbol{\rho}_e^{(l)}[n]$, $\iota_o(\mathbf{E}[n], \boldsymbol{\rho}^{(l)}[n])$, $\varsigma_o(\mathbf{A}_s[n], \boldsymbol{\rho}^{(l)}[n])$, and $\tau_o^{(l)}[n]$ are shown in (32), (33), (34), and (35), respectively.

To maintain the accuracy of the approximation, we introduce a set of trust region constraints as

$$\|\boldsymbol{\rho}^{(l)}[n] - \boldsymbol{\rho}^{(l-1)}[n]\| \leq \psi^{(l)}, \forall n \in \mathcal{N}, \quad (36)$$

where $\psi^{(l)}$ represents the trust region's radius. Notably, theoretically, reduce the radius $\psi^{(l)}$ to a sufficiently small value, which guarantees the convergence of the iterative procedure.

Ultimately, by substituting the non-concave objective function of problem (P4) and the non-convex constraints (23a) and

(23b) with their respective approximate forms as given in (29), (30), and (31), and incorporating the trust region constraints in (36), we derive the convex approximation of problem (P4) in the l -th iteration as follows, which can be efficiently solved using CVX.

$$(P5.l) : \max_{\{\boldsymbol{\rho}[n]\}} \frac{1}{N} \sum_{n=1}^N \bar{R}_s^{(l)}[n] \quad (37)$$

s.t. (1), (2), (30), (31), (36).

To sum up, we solve for the communication beamforming vectors $\{\mathbf{b}[n]\}$, the sensing covariance matrices $\{\mathbf{A}_s[n]\}$ and the UAV trajectory $\{\boldsymbol{\rho}[n]\}$ in an alternating manner. Since both subproblems can be guaranteed to converge, we finally obtain an efficient solution to problem (P1).

IV. NUMERICAL RESULTS

In this section, we present numerical results to assess the effectiveness of the proposed algorithm. Unless stated otherwise, the simulation settings are as follows: $\boldsymbol{\rho}_I = [300, 400, 200]^T$ m, $\boldsymbol{\rho}_F = [300, 600, 200]^T$ m, $\mathbf{s}_t = [250, 480, 0]^T$ m, $\mathbf{s}_u = [250, 520, 0]^T$ m, $\mathbf{s}_e = [350, 500, 0]^T$ m, $T = 12$ s, $v_{\max} = 25$ m/s, $M = 4$, $\Gamma_t = \Gamma_e = 10^{-6}$, $P_{\max} = 1$ W, $\beta_0 = -30$ dBm, and $\sigma^2 = -90$ dBm. To facilitate comparison, we evaluate three baseline approaches as follows.

- **Straight-flight trajectory with beamforming optimization:** The UAV adopts the straight-flight trajectory, traveling at a uniform speed $\|\boldsymbol{\rho}_I - \boldsymbol{\rho}_F\|/T$ from the starting position to the destination. Based on the straight-flight trajectory, the UAV dynamically adjusts the transmit information and sensing beamforming by solving problem (P2).
- **Trajectory design with constant beamforming:** The UAV optimizes the trajectory by solving problem (P4) with a simple maximum ratio transmission information beamforming with $\mathbf{b}[n] = \sqrt{\min(P_{\max}, P_c)} \mathbf{g}_u(\boldsymbol{\rho}[n]) / \|\mathbf{g}_u(\boldsymbol{\rho}[n])\|$, $\forall n \in \mathcal{N}$, in which P_c is the maximum transmission power that satisfies the sensing security threshold at the eavesdropper.
- **Benchmark without sensing security:** The UAV jointly optimizes its trajectory and the beamforming in problem (P1) by ignoring the sensing security constraint (13d).

Fig. 2 compares the trajectory obtained by our proposed design and the benchmark without sensing security. In both schemes, the UAV is observed to follow arc-like paths that

$$\boldsymbol{\rho}_o^{(l)}[n] = \frac{\log_e e}{\eta_o(\mathbf{E}[n], \boldsymbol{\rho}^{(l)}[n])} \iota_o(\mathbf{E}[n], \boldsymbol{\rho}^{(l)}[n]) (\boldsymbol{\rho}^{(l)}[n] - \mathbf{s}_o) - \frac{\log_e e}{\xi_o(\mathbf{A}_s[n], \boldsymbol{\rho}^{(l)}[n])} \varsigma_o(\mathbf{A}_s[n], \boldsymbol{\rho}^{(l)}[n]) (\boldsymbol{\rho}^{(l)}[n] - \mathbf{s}_o), o \in \{u, e, t\}. \quad (32)$$

$$\iota_o(\mathbf{E}[n], \boldsymbol{\rho}^{(l)}[n]) = \sum_{i=1}^M \sum_{j=i+1}^M 2\pi |[\mathbf{E}[n]]_{i,j}| \sin\left(\theta_{i,j}^{\mathbf{E}}[n] + \frac{\pi(j-i)D}{d_o(\boldsymbol{\rho}^{(l)}[n])}\right) \frac{(j-i)D}{d_o^3(\boldsymbol{\rho}^{(l)}[n])} + \frac{2\sigma^2}{\beta_0}, o \in \{u, e, t\}. \quad (33)$$

$$\varsigma_o(\mathbf{A}_s[n], \boldsymbol{\rho}^{(l)}[n]) = \sum_{i=1}^M \sum_{j=i+1}^M 2\pi |[\mathbf{A}_s[n]]_{i,j}| \sin\left(\theta_{i,j}^{\mathbf{A}_s}[n] + \frac{\pi(j-i)D}{d_o(\boldsymbol{\rho}^{(l)}[n])}\right) \frac{(j-i)D}{d_o^3(\boldsymbol{\rho}^{(l)}[n])} + \frac{2\sigma^2}{\beta_0}, o \in \{u, e, t\}. \quad (34)$$

$$\tau_o^{(l)}[n] = \sum_{i=1}^M \sum_{j=i+1}^M 2\pi |[\mathbf{E}[n]]_{i,j}| \sin\left(\theta_{i,j}^{\mathbf{E}}[n] + \frac{\pi(j-i)D}{d_o(\boldsymbol{\rho}^{(l)}[n])}\right) \frac{(j-i)D}{d_o^3(\boldsymbol{\rho}^{(l)}[n])} (\boldsymbol{\rho}^{(l)}[n] - \mathbf{s}_o), o \in \{u, e, t\}. \quad (35)$$

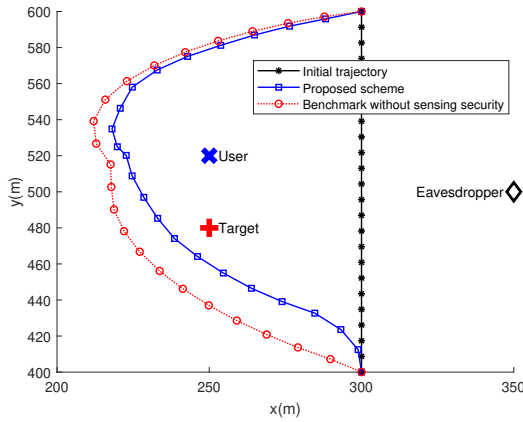


Fig. 2: Trajectories obtained by our proposed design and the benchmark without sensing security.

move towards the legitimate user and target while avoiding the eavesdropper, in order to prevent information and sensing leakage. It is also observed that the trajectory obtained by the proposed design is closer to the legitimate nodes. This is because when sensing security is considered, most of the power is concentrated in the communication signal and reused for target sensing as shown in Fig. 3. Compared to the benchmark without sensing security, the beam is not as focused, so the UAV needs to be closer to the two legitimate nodes in order to cover both.

Fig. 4 presents the beam pattern gain at time slot 10 in space by our proposed design and the benchmark without sensing security. It is observed that both the user and target are within the high-gain region, while the eavesdropper is located in the low-gain region, thus ensuring communication and sensing security. It is also observed that by comparing the two sub-figures, the SINR and beam pattern gain of the user and eavesdropper under the benchmark without sensing security are higher than those of the proposed design. When sensing security is not considered, the primary objective focuses on enhancing the disparity in the rate between the legitimate and eavesdropping channels to enhance the secrecy rate. This results in a higher secrecy rate but also introduces potential sensing security vulnerabilities, which aligns with the findings

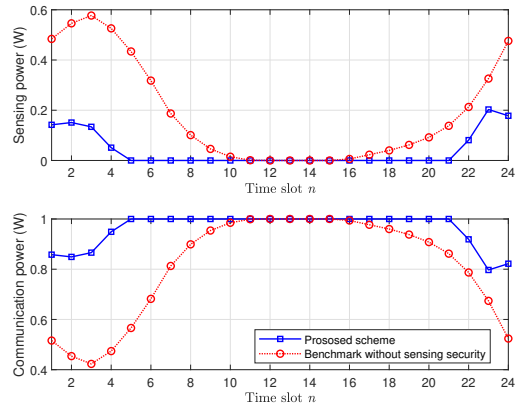


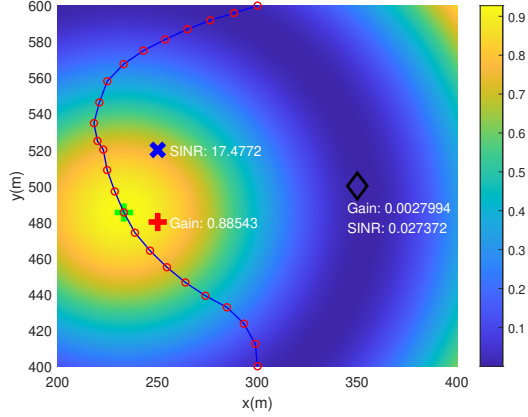
Fig. 3: Power allocation between sensing and communication signals over time by our proposed design and the benchmark without sensing security.

in Fig. 2.

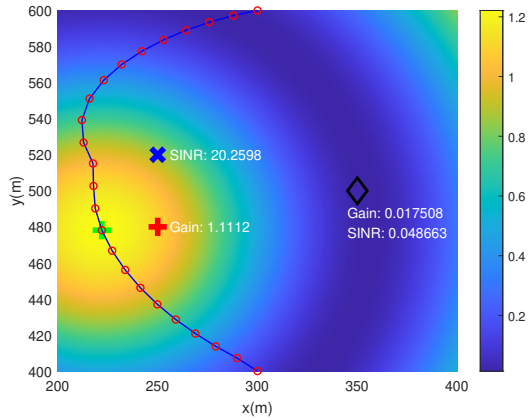
Fig. 5 illustrates the relationship between the antenna number M and the average secrecy rate. It is observed that the average secrecy rate achieved by all four schemes increases as the antenna number grows, since additional antennas provide more degrees of freedom and array gains. It is also observed that our proposed scheme significantly outperforms the straight-flight trajectory with beamforming optimization scheme and trajectory design with constant beamforming scheme. Additionally, the gap in secrecy rate between our proposed design and the benchmark without sensing security highlights the rate penalty associated with ensuring secure transmission against sensing eavesdropping.

V. CONCLUSION

This work considered a UAV-enabled secure ISAC system, where an aerial dual-functional BS simultaneously performs secure communication with a communication user and performs radar sensing of a target, in the presence of an eavesdropper intercepting both information and sensing. We focused on maximizing the average achievable secrecy rate through the optimization of the UAV trajectory, as well as the transmit information and sensing beamforming. How to extend

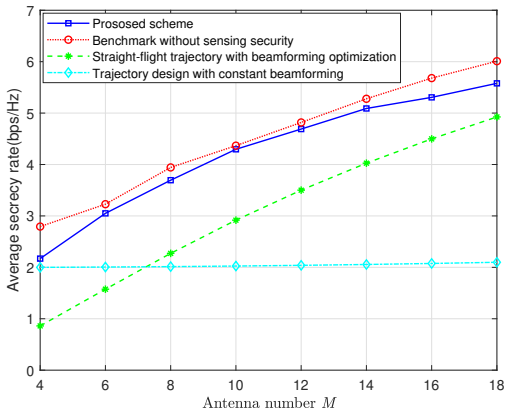


(a) Proposed scheme



(b) Benchmark without sensing security

Fig. 4: Achieved beam pattern gain at time slot 10.

Fig. 5: Average secrecy rate versus the antenna number M .

our approach to other configurations, such as multiple users, presents promising avenues for future research.

APPENDIX A PROOF OF LEMMA 1

With the obtained solution $\mathbf{B}^*[n]$ and $\mathbf{A}_s^*[n]$ to problem (P3), we can construct the follow solutions, shown as

$$\bar{\mathbf{b}}[n] = \frac{\mathbf{B}^*[n]\mathbf{g}_u(\boldsymbol{\rho}[n])}{\sqrt{\mathbf{g}_u^H(\boldsymbol{\rho}[n])\mathbf{B}^*[n]\mathbf{g}_u(\boldsymbol{\rho}[n])}}, \quad (38)$$

$$\bar{\mathbf{B}}[n] = \bar{\mathbf{b}}[n]\bar{\mathbf{b}}^H[n], \quad (39)$$

$$\bar{\mathbf{A}}_s[n] = \mathbf{B}^*[n] + \mathbf{A}_s^*[n] - \bar{\mathbf{B}}[n]. \quad (40)$$

In the following, we will prove that the new constructed solution $\bar{\mathbf{B}}[n]$ and $\bar{\mathbf{A}}_s[n]$ is feasible for problem (P3) with the same objective value as that of the solution $\mathbf{B}^*[n]$ and $\mathbf{A}_s^*[n]$. We can easy get that $\bar{\mathbf{B}}[n]$ is positive semidefinite and rank-one. Next, we will show that $\bar{\mathbf{A}}_s[n]$ is also positive semidefinite.

For any $\mathbf{w} \in \mathbb{C}^{M \times 1}$, it holds that

$$\begin{aligned} & \mathbf{w}^H (\mathbf{B}^*[n] - \bar{\mathbf{B}}[n]) \mathbf{w} \\ &= \mathbf{w}^H \mathbf{B}^*[n] \mathbf{w} - |\mathbf{w}^H \mathbf{B}^*[n] \mathbf{g}_u(\boldsymbol{\rho}[n])|^2 \\ & \quad (\mathbf{g}_u^H(\boldsymbol{\rho}[n]) \mathbf{B}^*[n] \mathbf{g}_u(\boldsymbol{\rho}[n]))^{-1}. \end{aligned} \quad (41)$$

According to the Cauchy-Schwarz inequality, we have

$$\begin{aligned} & |\mathbf{w}^H \mathbf{B}^*[n] \mathbf{g}_u(\boldsymbol{\rho}[n])|^2 (\mathbf{g}_u^H(\boldsymbol{\rho}[n]) \mathbf{B}^*[n] \mathbf{g}_u(\boldsymbol{\rho}[n]))^{-1} \\ &= |\mathbf{w}^H \bar{\mathbf{b}}^*[n] \bar{\mathbf{b}}^{*H}[n] \mathbf{g}_u(\boldsymbol{\rho}[n])|^2 (\mathbf{g}_u^H(\boldsymbol{\rho}[n]) \mathbf{B}^*[n] \mathbf{g}_u(\boldsymbol{\rho}[n]))^{-1} \\ &\leq |\mathbf{w}^H \bar{\mathbf{b}}^*[n]|^2 |\mathbf{g}_u^H(\boldsymbol{\rho}[n]) \bar{\mathbf{b}}^*[n]|^2 (\mathbf{g}_u^H(\boldsymbol{\rho}[n]) \mathbf{B}^*[n] \mathbf{g}_u(\boldsymbol{\rho}[n]))^{-1} \\ &= \mathbf{w}^H \bar{\mathbf{b}}^*[n] \bar{\mathbf{b}}^{*H}[n] \mathbf{w} \\ &= \mathbf{w}^H \mathbf{B}^*[n] \mathbf{w}. \end{aligned} \quad (42)$$

Thus, we have

$$\mathbf{w}^H (\mathbf{B}^*[n] - \bar{\mathbf{B}}[n]) \mathbf{w} \geq 0. \quad (43)$$

According to (43), we have $\mathbf{B}^*[n] - \bar{\mathbf{B}}[n] \succeq 0$. Based on this fact together with $\bar{\mathbf{A}}_s^*[n] \succeq 0$, it follows that $\bar{\mathbf{A}}_s[n] = \mathbf{B}^*[n] + \mathbf{A}_s^*[n] - \bar{\mathbf{B}}[n]$ should be positive semidefinite.

In addition, we need to prove that substituting the reconstructed solution $\bar{\mathbf{B}}[n]$ and $\bar{\mathbf{A}}_s[n]$ into the original problem still yields the same objective function value satisfying the corresponding constraints (14b), (14c), and (14d). The proof is shown as follows.

$$\begin{aligned} & \Phi_t^H(\boldsymbol{\rho}[n])(\bar{\mathbf{B}}[n] + \bar{\mathbf{A}}_s[n])\Phi_t(\boldsymbol{\rho}[n]) \\ &= \Phi_t^H(\boldsymbol{\rho}[n])(\bar{\mathbf{B}}[n] + \mathbf{B}^*[n] + \mathbf{A}_s^*[n] - \bar{\mathbf{B}}[n])\Phi_t(\boldsymbol{\rho}[n]) \\ &= \Phi_t^H(\boldsymbol{\rho}[n])(\mathbf{B}^*[n] + \mathbf{A}_s^*[n])\Phi_t(\boldsymbol{\rho}[n]) \geq \Gamma_t d_t^2(\boldsymbol{\rho}[n]), \end{aligned} \quad (44)$$

$$\begin{aligned} & \Phi_e^H(\boldsymbol{\rho}[n])(\bar{\mathbf{B}}[n] + \bar{\mathbf{A}}_s[n])\Phi_e(\boldsymbol{\rho}[n]) \\ &= \Phi_e^H(\boldsymbol{\rho}[n])(\bar{\mathbf{B}}[n] + \mathbf{B}^*[n] + \mathbf{A}_s^*[n] - \bar{\mathbf{B}}[n])\Phi_e(\boldsymbol{\rho}[n]) \\ &= \Phi_e^H(\boldsymbol{\rho}[n])(\mathbf{B}^*[n] + \mathbf{A}_s^*[n])\Phi_e(\boldsymbol{\rho}[n]) \leq \Gamma_e d_e^2(\boldsymbol{\rho}[n]), \end{aligned} \quad (45)$$

$$\begin{aligned}
& \text{tr}(\bar{\mathbf{B}}[n]) + \text{tr}(\bar{\mathbf{A}}_s[n]) \\
&= \text{tr}(\bar{\mathbf{B}}[n] + \bar{\mathbf{A}}_s[n]) \\
&= \text{tr}(\bar{\mathbf{B}}[n] + \mathbf{B}^*[n] + \mathbf{A}_s^*[n] - \bar{\mathbf{B}}[n]) \\
&= \text{tr}(\mathbf{B}^*[n] + \mathbf{A}_s^*[n]) \\
&= \text{tr}(\mathbf{B}^*[n]) + \text{tr}(\mathbf{A}_s^*[n]) \leq P_{\max}. \tag{46}
\end{aligned}$$

For the prove about the objective function, we can first derive the following equations

$$\begin{aligned}
& \mathbf{g}_u^H(\boldsymbol{\rho}[n])\bar{\mathbf{B}}[n]\mathbf{g}_u(\boldsymbol{\rho}[n]) \\
&= \mathbf{g}_u^H(\boldsymbol{\rho}[n])\bar{\mathbf{b}}[n]\bar{\mathbf{b}}^H[n]\mathbf{g}_u(\boldsymbol{\rho}[n]) \\
&= \mathbf{g}_u^H(\boldsymbol{\rho}[n])\mathbf{B}^*[n]\mathbf{g}_u(\boldsymbol{\rho}[n]), \tag{47}
\end{aligned}$$

$$\begin{aligned}
& \mathbf{g}_e^H(\boldsymbol{\rho}[n])\bar{\mathbf{B}}[n]\mathbf{g}_e(\boldsymbol{\rho}[n]) \\
&= \mathbf{g}_e^H(\boldsymbol{\rho}[n])\bar{\mathbf{b}}[n]\bar{\mathbf{b}}^H[n]\mathbf{g}_e(\boldsymbol{\rho}[n]) \\
&= \mathbf{g}_e^H(\boldsymbol{\rho}[n])\mathbf{B}^*[n]\mathbf{g}_e(\boldsymbol{\rho}[n]). \tag{48}
\end{aligned}$$

For the first two terms of Eq. (15), it can be rewritten as

$$\begin{aligned}
& \log_2(\text{tr}(\mathbf{g}_u(\boldsymbol{\rho}[n])\mathbf{g}_u^H(\boldsymbol{\rho}[n])\bar{\mathbf{B}}[n]) \\
&+ \text{tr}(\mathbf{g}_u(\boldsymbol{\rho}[n])\mathbf{g}_u^H(\boldsymbol{\rho}[n])\bar{\mathbf{A}}_s[n]) + \sigma^2) \\
&+ \log_2(\text{tr}(\mathbf{g}_e(\boldsymbol{\rho}[n])\mathbf{g}_e^H(\boldsymbol{\rho}[n])\bar{\mathbf{A}}_s[n]) + \sigma^2) \\
&= \log_2(\text{tr}(\mathbf{g}_u(\boldsymbol{\rho}[n])\mathbf{g}_u^H(\boldsymbol{\rho}[n])\bar{\mathbf{B}}[n]) \\
&+ \text{tr}(\mathbf{g}_u(\boldsymbol{\rho}[n])\mathbf{g}_u^H(\boldsymbol{\rho}[n])(\mathbf{B}^*[n] + \mathbf{A}_s^*[n] - \bar{\mathbf{B}}[n])) + \sigma^2) \\
&+ \log_2(\text{tr}(\mathbf{g}_e(\boldsymbol{\rho}[n])\mathbf{g}_e^H(\boldsymbol{\rho}[n])(\mathbf{B}^*[n] + \mathbf{A}_s^*[n] - \bar{\mathbf{B}}[n])) + \sigma^2) \\
&= \log_2(\text{tr}(\mathbf{g}_u(\boldsymbol{\rho}[n])\mathbf{g}_u^H(\boldsymbol{\rho}[n])\mathbf{B}^*[n]) \\
&+ \text{tr}(\mathbf{g}_u(\boldsymbol{\rho}[n])\mathbf{g}_u^H(\boldsymbol{\rho}[n])\mathbf{A}_s^*[n]) + \sigma^2) \\
&+ \log_2(\text{tr}(\mathbf{g}_e(\boldsymbol{\rho}[n])\mathbf{g}_e^H(\boldsymbol{\rho}[n])\mathbf{A}_s^*[n]) + \sigma^2). \tag{49}
\end{aligned}$$

Similarly, for the last two terms of Eq. (15), it can be reformulated as

$$\begin{aligned}
& (\delta_u^{(l)}[n] + \text{tr}(\Lambda_u^{(l)}[n](\bar{\mathbf{A}}_s[n] - \mathbf{A}_s^{(l)}[n]))) \\
&+ (\delta_e^{(l)}[n] + \text{tr}(\Lambda_e^{(l)}[n](\bar{\mathbf{B}}[n] - \mathbf{B}^{(l)}[n])) \\
&+ \text{tr}(\Lambda_e^{(l)}[n](\bar{\mathbf{A}}_s[n] - \mathbf{A}_s^{(l)}[n])) \\
&= (\delta_u^{(l)}[n] + \text{tr}(\Lambda_u^{(l)}[n](\mathbf{B}^*[n] + \mathbf{A}_s^*[n] - \bar{\mathbf{B}}[n] - \mathbf{A}_s^{(l)}[n]))) \\
&+ (\delta_e^{(l)}[n] + \text{tr}(\Lambda_e^{(l)}[n](\bar{\mathbf{B}}[n] - \mathbf{B}^{(l)}[n])) \\
&+ \text{tr}(\Lambda_e^{(l)}[n](\mathbf{B}^*[n] + \mathbf{A}_s^*[n] - \bar{\mathbf{B}}[n] - \mathbf{A}_s^{(l)}[n])) \\
&= (\delta_u^{(l)}[n] + \text{tr}(\Lambda_u^{(l)}[n](\mathbf{A}_s^*[n] - \mathbf{A}_s^{(l)}[n]))) \\
&+ (\delta_e^{(l)}[n] + \text{tr}(\Lambda_e^{(l)}[n](\mathbf{B}^*[n] - \mathbf{B}^{(l)}[n])) \\
&+ \text{tr}(\Lambda_e^{(l)}[n](\mathbf{A}_s^*[n] - \mathbf{A}_s^{(l)}[n])). \tag{50}
\end{aligned}$$

By combining (49) and (50), it is evident that the objective value remains the same.

This completes the proof.

REFERENCES

- [1] F. Liu, Y. Cui, C. Masouros, J. Xu, T. Han, Y. Eldar, and S. Buzzi, "Integrated sensing and communications: Toward dual-functional wireless networks for 6G and beyond," *IEEE J. Sel. Areas Commun.*, vol. 40, no. 6, pp. 1728-1767, Mar. 2022.
- [2] A. Liu, Z. Huang, M. Li, Y. Wan, et al., "A survey on fundamental limits of integrated sensing and communication," *IEEE Commun. Surveys Tuts.*, vol. 24, no. 2, pp. 994-1034, Second Quarter, 2022.
- [3] Z. Lyu, G. Zhu, and J. Xu, "Joint maneuver and beamforming design for UAV-enabled integrated sensing and communication," *IEEE Trans. Wireless Commun.*, vol. 22, no. 4, pp. 2424-2440, Oct. 2022.
- [4] K. Meng, Q. Wu, J. Xu, W. Chen, Z. Feng, and R. Schober, "UAV-enabled integrated sensing and communication: Opportunities and challenges," *IEEE Wireless Commun.*, vol. 31, no. 2, pp. 97-104, Apr. 2024.
- [5] C. Zhong, J. Yao, and J. Xu, "Secure UAV communication with cooperative jamming and trajectory control," *IEEE Commun. Lett.*, vol. 23, no. 2, pp. 286-289, Feb. 2019.
- [6] M. Hua, Q. Wu, W. Chen, O. Dobre, and A. Swindlehurst, "Secure intelligent reflecting surface-aided integrated sensing and communication," *IEEE Trans. Wireless Commun.*, vol. 23, no. 1, pp. 575-591, Jan. 2024.
- [7] Z. Ren, L. Qiu, J. Xu and D. W. K. Ng, "Robust transmit beamforming for secure integrated sensing and communication," *IEEE Trans. Commun.*, vol. 71, no. 9, pp. 5549-5564, Sep. 2023.
- [8] N. Su, F. Liu, and C. Masouros, "Sensing-assisted eavesdropper estimation: An ISAC breakthrough in physical layer security," *IEEE Trans. Wireless Commun.*, vol. 23, no. 4, pp. 3162-3174, Apr. 2024.
- [9] J. Zou, C. Masouros, F. Liu, and S. Sun, "Securing the sensing functionality in ISAC networks: An artificial noise design," *IEEE Trans. Veh. Tech.*, vol. 73, no. 11, pp. 17800-17805, Nov. 2024.
- [10] Z. Ren, J. Xu, L. Qiu, and D. W. K. Ng, "Secure cell-free integrated sensing and communication in the presence of information and sensing eavesdroppers," *IEEE J. Sel. Areas Commun.*, vol. 42, no. 11, pp. 3217-3231, Nov. 2024.
- [11] X. Liu, T. Huang, N. Shlezinger, Y. Liu, J. Zhou and Y. C. Eldar, "Joint transmit beamforming for multiuser MIMO communications and MIMO radar," *IEEE Trans. Signal Process.*, vol. 68, pp. 3929-3944, Jun. 2020.